

Finite-Time Optimization of Quantum Szilard heat engine

Tan-Ji Zhou,^{1,2} Yu-Han Ma,^{3,1,*} and C. P. Sun^{1,4,†}

¹Graduate School of China Academy of Engineering Physics,
No. 10 Xibeiwang East Road, Haidian District, Beijing, 100193, China

²Department of Physics, Peking University

³Department of Physics, Beijing Normal University, Beijing 100875, China

⁴Beijing Computational Science Research Center, Beijing 100193, China

We propose a finite-time quantum Szilard engine (QSE) with a quantum particle with spin as the working substance (WS) to accelerate the operation of information engines. A Maxwell's demon (MD) is introduced to probe the spin state within a finite measurement time t_M to capture the which-way information of the particle, quantified by the mutual information $I(t_M)$ between WS and MD. We establish that the efficiency η of QSE is bounded by $\eta \leq 1 - (1 - \eta_C) \ln 2 / I(t_M)$, where $I(t_M) / \ln 2$ characterizes the ideality of quantum measurement, and approaches 1 for the Carnot efficiency reached under ideal measurement in quasi-static regime. We find that the power of QSE scales as $P \propto t_M^3$ in the short-time regime and as $P \propto t_M^{-1}$ in the long-time regime. Additionally, considering the energy cost for erasing the MD's memory required by Landauer's principle, there exists a threshold time that guarantees QSE to output positive work.

Introduction.—The field of information heat engines [1, 2] was developed to establish the fundamental role of information in thermodynamics [2, 3]. These engines operate by generating work through information processing, rather than conventional heat absorption. A well-known example is the Szilard engine [1], which involves the Maxwell's demon (MD) probing the position of particles in a single heat reservoir to extract work. The apparent violation of the second law of thermodynamics in this case is resolved [2–7] by taking into account the energy cost of erasing the demon's memory, as per Landauer's principle [8]. Several quantum Szilard engines (QSEs) have been proposed [2–7] to explore the connection between information and thermodynamics in quantum regime.

In QSEs, the demon's recording of the particle's position is equivalent to the establishment of entanglement between MD and the particle. However, high-speed cyclic operation needs to be accomplished within a short measurement time to achieve optimal power of QSE. This makes it impossible to carry out an ideal quantum measurement, according to the decoherence theory for quantum measurement [9–12].

In this Letter, we propose and study a finite-time QSE model to analyze the influence of non-ideal quantum measurement on engine performance. We investigate the information correlation between the particle and MD during quantum measurement and analyze the dynamics of the which-way information recorded by MD. Our results demonstrate the fundamental trade-off between the power and efficiency of QSE due to non-ideal measurement. Although information recording does not consume additional energy, the non-ideality of measurement affects the thermodynamic signatures of the QSE.

Operation cycle of a QSE.—As illustrated in Fig. 1, the working substance (WS) of the considered QSE is specified as a single particle with spin-1/2. The MD probes the particle's position through the detection of its spin state to obtain the which-way information of the particle, which can be further used to output work. The operation cycle of the QSE involves three stages, namely, information recording through quantum measurement (stage I), work outputting (stage II) and information erasing (stage III).

In stage I, the particle is injected into a cylinder, and the inhomogeneous magnetic field which perpendicular to the direction of the particle's incidence is turned on. This results in the entanglement of the particle's spin and spatial states, enabling the Maxwell's demon to detect the particle's position through measurement of its spin state.

After stage I, the spin-magnetic field interaction gives rise to a time-dependent correlation $I(t_M)$ between the spin state and the spatial state, and the deflection of the particle can be inferred from the spin detection. Hereafter, the duration of stage I t_M is called the measurement time. We qualify such correlation with the mutual information [13] as

$$I(t_M) = I_{DP} \equiv S_D + S_p - S_{DP}, \quad (1)$$

where S_{DP} , S_D and S_p are the Shannon entropy of the total system, the MD and the particle, respectively.

In stage II, the magnetic field is turned off and a suitable protocol is chosen according to MD's memory to enable the extraction of work from collisions of the particle and baffle. The engine is contacting with a heat reservoir with temperature T_H when it outputs work. At the end of stage II, the correlation between the particle and MD vanished due to their thermalization in the reservoir, thereby contributing to an increase of their total entropy, i.e., $\Delta S_{DP} = I(t_M)$ [14, 15].

* yhma@bnu.edu.cn

† suncp@gscaep.ac.cn

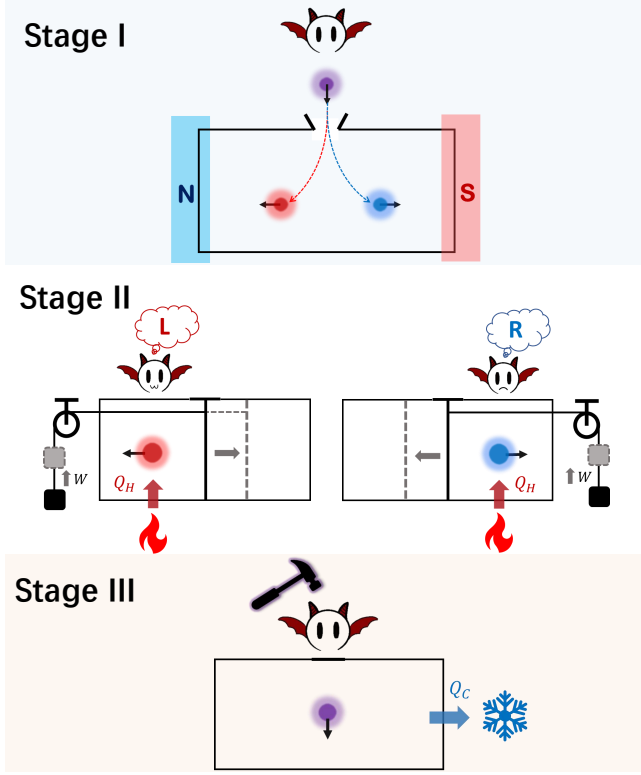


Figure 1. Schematic illustration of the Szilard engine cycle. MD first observes the position of the particle (through the detection of the particle's spin) in the box (stage I). Then proper operation is chosen to extract work from collisions of particle and baffle (stage II). After the work done process, the information of the particle's position recorded by MD is erased, and the entire system returns to its initial state (stage III).

The generalized free energy [15–20] of the total system containing the particle and MD

$$F \equiv U - k_B T_H S_{DP} \quad (2)$$

is defined by Shannon entropy S_{DP} instead of the thermodynamic entropy in conventional cases. Here, U is the energy of the total system. Consequently, it follows from Eq. (2) and the 2nd law of thermodynamics ($W \leq -\Delta F$) that the output work is bounded above by the spin-position correlation of the particle as

$$W_O \leq k_B T_H I(t_M), \quad (3)$$

where the facts that the internal energy of an ideal gas particle is unchanged in the isothermal process and MD's energy remains unchanged throughout the whole cycle have been used. As a result, heat in the amount of $Q_O = W_O$ is absorbed from the heat reservoir.

In stage III, the information recorded by MD is erased, and the entire system returns to its initial state. In this process, the engine is in contact with another

reservoir with temperature T_C . According to Landauer's principle, work in the amount of $W_E \geq k_B T_C \ln 2$ must be applied to the system [8] to erase MD's memory (to initialize the spin state in our case). The same amount of heat $Q_E = W_E$ is dissipated into the reservoir according to the first law of thermodynamics in this isothermal process.

Realization of the cycle.—Taken Stern-Gerlach experiment [21–24] as an realization of stage I, the correlation between spin state and the spatial state of the particle can be specifically obtained (See Sec. I of the Supplementary Materials (SM) for details [25]). We define the measurement ideality as $\mathcal{M} \equiv I/\ln 2$ and it is explicitly written as [25]

$$\mathcal{M}(\tilde{t}) = 1 + \frac{p(\tilde{t}) \ln p(\tilde{t}) + [1 - p(\tilde{t})] \ln [1 - p(\tilde{t})]}{\ln 2} \quad (4)$$

with

$$p(\tilde{t}) = \frac{1}{2} \left[1 + \operatorname{erf} \left(\frac{\alpha \tilde{t}^2}{\sqrt{2\tilde{t}^2 + 8}} \right) \right] \quad (5)$$

the possibility that MD can accurately infer the particle's position. Here, $\operatorname{erf}(z) = 2\pi^{-1/2} \int_0^z \exp(-u^2) du$ is the Gaussian error function, $\tilde{t} \equiv t_M/\tau_M$ is the dimensionless measurement time. The characteristic time of the measurement process $\tau_M \equiv ma^2/\hbar$ is determined by the particle mass m and the width of the particle's spatial wave packet a . In addition, $\alpha \equiv ma^3 f/\hbar^2$ is proportional to the magnetic force f acting on the spin.

We further plot $\mathcal{M}(\tilde{t})$ as a function of \tilde{t} in Fig. 2(a). It is clearly seen in this figure that for a given measurement time, larger α results in a greater degree of correlation generated between the spin degrees of freedom and the spatial degrees of freedom of the particle, and thus MD can more accurately distinguish the position of the particle. As the measurement time increases, the spin-position correlation of the particle monotonically increases. In the ideal measurement process, we have $\lim_{\tilde{t} \rightarrow \infty} \mathcal{M}(\tilde{t}) = 1$ ($p(\tilde{t}) \rightarrow 1$), which is the plateau approached by the three curves in Fig. 2(a).

We emphasize here that the essential difference between the Szilard engine with finite-time quantum measurement proposed in this work and the conventional one is reflected in the maximum extracted work allowed by the information recording process. In the conventional Szilard engine, MD can deterministically observe the position of the particle, enabling a precise judgment on which operation to choose to extract work. However, in our case, the dynamics of the measurement renders the inference of the particle's position from its spin state probabilistic. The possibility of selecting an incorrect operation for extracting work will reduce the output work, which has been recently discussed for the correlated variable Szilard engine in non-dynamical case [15].

In particular, $\tilde{t} \rightarrow 0$ is associated with invalid measurement with $\mathcal{M} \rightarrow 0$. Consequently, MD knows nothing

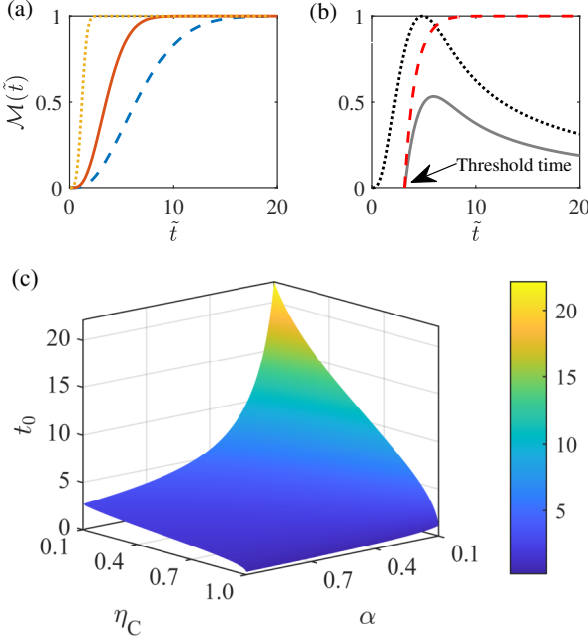


Figure 2. (a) Measurement ideality $\mathcal{M}(t) = I(t)/\ln 2$ with different α . The blue dashed curve, orange solid curve, and yellow dotted curve are plotted with $\alpha = 0.2$, $\alpha = 0.4$, and $\alpha = 2$, respectively. (b) Efficiency and power of the engine as the function of dimensionalized measurement time, where $\eta_C = 0.6$, $\alpha = 0.4$ are used. The grey solid curve and the black dotted curve mark $P(\tilde{t})$ and $P_O(\tilde{t})$ respectively, which are normalized by $\max[P_O(\tilde{t})]$, and the red dashed line marks $\eta(\tilde{t})$ which is normalized by η_C . (c) The threshold time t_0 as a function of the Carnot efficiency η_C and the characteristic parameter $\alpha = ma^3 f/\hbar^2$. The yellow area corresponds to higher value of t_0 and the blue area corresponds to the lower part. t_0 is numerically solved from Eq. (10) for each given set of η_C and α .

about the particle's position, and thus no work can be extracted. On the other hand, when an ideal measurement with $\mathcal{M} = 1$ is achieved in the quasi-static regime ($\tilde{t} \rightarrow \infty$), Eq. (3) recovers the result $W_O^{\text{ideal}} = k_B T_H \ln 2$ of the conventional Szilard engine. Hence we can rewrite the upper bound of the outputting work in Eq. (3) as $W_O \leq \mathcal{M}W_O^{\text{ideal}}$.

Efficiency and power of the QSE.—With the energy conversion relations in the above cycle analysis in mind, the total work of the QSE performing in one cycle reads

$$W = W_O - W_E \leq \mathcal{M}W_O^{\text{ideal}} - k_B T_C \ln 2, \quad (6)$$

and thus the efficiency of the QSE $\eta \equiv W/Q_O = W/W_O$ satisfies

$$\eta \leq 1 - \frac{k_B T_C \ln 2}{\mathcal{M}W_O^{\text{ideal}}} = 1 - \frac{(1 - \eta_C)}{\mathcal{M}}. \quad (7)$$

The above inequality can be reorganized in terms of the Carnot efficiency $\eta_C \equiv 1 - T_C/T_H$ as

$$\frac{1 - \eta_C}{1 - \eta} \leq \mathcal{M}, \quad (8)$$

which is the main result of this Letter, revealing fundamental upper bound on energy conversion efficiency set by information measurement ideality. Here, the equal sign is saturated if and only if there is no irreversibility in stage II and stage III.

By definition, the power of the QSE is $P \equiv W/t_{\text{cycle}}$, where the cycle time is $t_{\text{cycle}} = t_M + t_O + t_E$ with the duration of the work outputting (information erasing) process to be t_O (t_E). In order to significantly demonstrate the impact of finite-time measurements on the performance of QSE, we first consider that the coupling between the system and measurement instrument is weak enough so that the finite-time behavior of the information recording dominates in the considered time scale ($t_E, t_O \ll t_M$) [25]. In this case, the irreversibility of the work outputting and information erasing processes can be ignored, and the power of the engine reduces to

$$P = \frac{W}{t_M} \leq \frac{\mathcal{M}W_O^{\text{ideal}} - k_B T_C \ln 2}{t_M} = \frac{\eta(\tilde{t})k_B T_H I(\tilde{t})}{\tau_M \tilde{t}}. \quad (9)$$

We further define the output power associated with the work outputting process as $P_O(\tilde{t}) \equiv W_O/t_M = k_B T_H I(\tilde{t})/(\tau_M \tilde{t})$, where the equal sign in Eq. (8) is taken.

We illustrate $\eta(\tilde{t})$, $P(\tilde{t})$, and $P_O(\tilde{t})$ as functions of non-dimensionalized measurement time \tilde{t} in Fig. 2 (b), where $P(\tilde{t})$ and $P_O(\tilde{t})$ are non-dimensionalized by the maximum value of $P_O(\tilde{t})$, and $\eta(\tilde{t})$ is normalized by η_C . As illustrated in this figure, $P_O(\tilde{t})$ increases from zero with the increase of measurement time \tilde{t} until it reaches its maximum value and then decreases gradually, which is positive for all $\tilde{t} > 0$. In the short time regime, $\mathcal{M}(\tilde{t}) \propto \alpha^2 \tilde{t}^4$ [25], and thus $P_O(\tilde{t} \ll 1) \propto \alpha^2 \tilde{t}^3$, which indicates the output power is proportional to the square of the strength of measurement (α^2). On the other hand, in the long time regime, $\mathcal{M}(\tilde{t})$ tends to 1 exponentially (see Fig. 2 (a)) such that $P_O(\tilde{t} \gg 1) \propto \tilde{t}^{-1}$.

Threshold time for positive work.—It is observed in Fig. 2 (b) that the power $P(\tilde{t})$ and the efficiency $\eta(\tilde{t})$ of the information heat engine are positive only when the time exceeds a threshold value. This can be understood from Eq. (6) that the positive work condition $W \geq 0$ sets a lower bound for measurement ideality as

$$\mathcal{M}(\tilde{t}) \geq 1 - \eta_C. \quad (10)$$

Naturally, we define the threshold time $t_0 \equiv \mathcal{M}^{-1}(1 - \eta_C)$ as the lower bound of the dimensionless measurement time that holds the above inequality. The positive work condition for the engine is thus converted to a restriction on the measurement time $\tilde{t} > t_0$.

For different value of η_C , the shape of the curves in Fig. 2 (b) will change on the premise that the overall

characteristics remain unchanged, resulting in different values of t_0 . We numerically solve t_0 from Eq. (10) for each given set of parameters $\{\eta_C \in (0.1, 1), \alpha \in (0.1, 1)\}$, and then plot t_0 as a function of η_C and α in Fig. 2 (c). This figure shows that the threshold time increase remarkably as α grows beyond a certain value, while it decreases rather gradually with the increase of η_C for relatively large α . Therefore, we can increase α to achieve a stronger measurement, thereby effectively reducing t_0 . By doing this, the engine can output positive work in a shorter cycle time. In other words, increasing α can speed up the engine operation without decreasing the output work, thereby improving the power of the engine.

Optimal operation of the QSE.— When the power of the information heat engine $P(\tilde{t})$ reaches its maximum at the measurement time $\tilde{t} = \tilde{t}^*$, i.e., $P(\tilde{t}^*) = \max\{P(\tilde{t})|\tilde{t} > 0\} \equiv P_{\max}$, the corresponding efficiency is referred to as the efficiency at maximum power (EMP). In Fig. 3 (a), the EMP of the engine η_{MP} as a function of η_C is plotted with the blue solid curve. The typical efficiency $\eta_+ = \eta_C/(2 - \eta_C)$, known as the upper bound of the EMP of low-dissipation Carnot heat engine [26], is marked with the orange dash-dotted curve. It can be observed from Fig. 3 that the EMP of QSE can exceed η_+ and finally approaches the Carnot efficiency $\eta_C = 1 - T_C/T_H$ (red dashed line) as $\eta_C \rightarrow 1$. In this example, $\alpha = 0.4$ is used. Note that η_+ is the overall upper bound for EMP of all near-equilibrium engines [27], the significantly higher EMP of our QSE indicates the quantum thermodynamical advantage away from equilibrium regime. In addition, the dependence of η_{MP}/η_C on α is shown in the inset figure, indicating that the EMP of QSE gradually increases with α and approaches the Carnot efficiency very closely.

Moreover, the power-efficiency trade-off relation [28–31] of our QSE is illustrated in Fig. 3 (b) with $\alpha = 0.4$ and $\eta_C = 0.6$. To obtain this trade-off, $P(\tilde{t})$ and $\eta(\tilde{t})$ are calculated numerically by varying the measurement time $\tilde{t} \in [1, 10^5]$. Increasing \tilde{t} results in an increase in η , while P first increases to reach its maximum value and then decreases, as shown in Fig. 2 (a). The EMP of the engine is associated with the rightmost edge of the curve (red squared dot), which is pointed by the red arrow. The maximum power P_{\max} as a function of α is demonstrated in the inset figure, which indicates that an increase in α will lead to a significant increase in P_{\max} .

Overall, the above obtained results demonstrate that the dynamics of information recording realized by quantum measurement has a significant impact on the operation of the Szilard engine. Specifically, more complete information recording (larger α) leads to higher maximum power as well as higher EMP of the engine.

Remarks on finite-time effects in stages II and III.— In the above discussion, only the finite-time behavior of the information recording process is taken into account. When we consider the finite-time effects in both the information recording and information erasing processes, we find that i) the EMP of the engine can also exceed

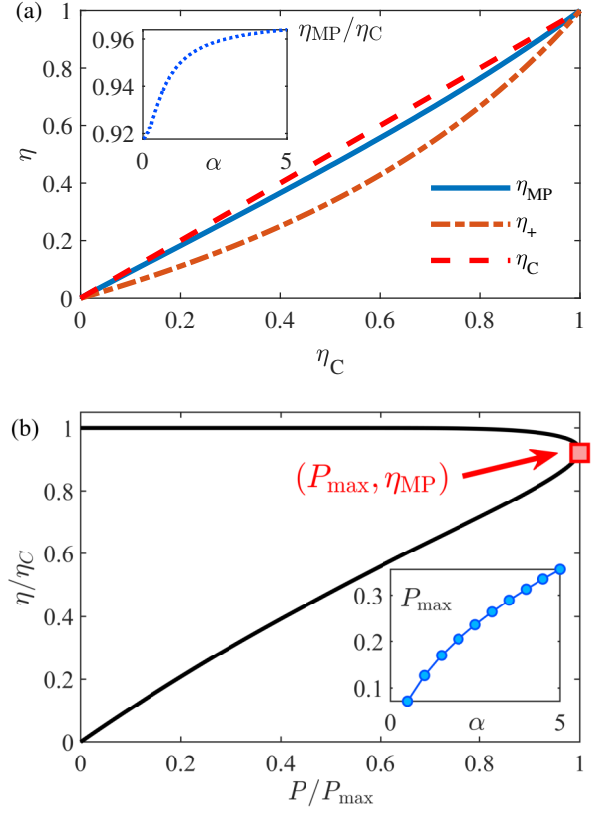


Figure 3. (a) Efficiency at maximum power of QSE as a function of η_C . The blue solid curve represents the efficiency at maximum power (EMP) of the information engine, the typical bound of EMP $\eta_+ = \eta_C/(2 - \eta_C)$ is plotted with the orange dash-dotted curve, and the red dashed line marks the Carnot efficiency $\eta_C = 1 - T_C/T_H$, in this plot $\alpha = 0.4$ is used. In the inset figure, EMP as a function of α is plotted with the blue dotted curve, and $\eta_C = 0.6$ is used. (b) Power-efficiency trade-off relation of QSE with $\alpha = 0.4$ and $\eta_C = 0.6$. In this figure, only the finite-time effect of the information recording process (stage I) is considered. In the inset figure, the maximum power P_{\max} as a function of α is plotted with the blue circle-dotted curve.

the upper limit of the efficiency of low-dissipation Carnot heat engine at a certain range of η_C ; ii) the QSE can operate anywhere within the envelop of the power-efficiency trade-off, which is quite different from the single-variable case shown in Fig. 3 (b) where the system can only operate with power and efficiency located on the curve. On the other hand, if the information recording is complete with an ideal measurement with $I(t_M) = \ln 2$, and the operation time of the measurement process can be ignored in comparison with that of the work outputting and information erasing process, then the information heat engine can be exactly mapped into a Carnot-like heat engine, whose EMP satisfies $\eta_C/2 \leq \eta_{\text{MP}} \leq \eta_C/(2 - \eta_C)$. The detailed calculations and discussion on these issues are given in Sec. II of the SM [25].

Conclusions and outlooks.—In summary, we propose a

finite-time quantum Szilard heat engine model. The non-ideal measurement of the working substance carried out by the demon allows the engine cycle to run fast with high power at the expense of efficiency. It is found that the engine is able to output positive work only after the measurement time reaches a threshold, which reflects the dynamic competition between the output work achieved by information recording and the work consumed for erasing information. The optimal performance of such information engine, characterized with the EMP and the power-efficiency trade-off relation, is obtained quantitatively. These results demonstrate that quantum measurements have potentially observable thermodynamic effects, which have a critical impact on thermodynamic cycles of exchanging information for energy.

This study bridges the gap between the dynamics of quantum measurement and non-equilibrium thermodynamics, and shall bring new insights in providing thermodynamic evidence for identifying different interpreta-

tions of quantum measurement [11, 32–35]. As potential extensions, the optimal control protocol [36, 37] and the geometric optimization [38, 39] of the cycle, the finite-sized effect of the reservoir [40–43] involved in the work output processes and erase process, the many-body effect of the working substance [44] are expected to be taken into future consideration. In addition, whether there is a thermodynamic criterion for objectivity in quantum measurement [11, 45–47] is a fundamental question worth exploring. Finally, inspired by the obtained results on thermodynamic signatures of information recording in quantum measurement, we leave a fascinating and challenging question to end this paper: *What thermodynamic consequences could be caused by the finite-time memory of intelligent life.*

Acknowledgment.—This work is supported by the National Natural Science Foundation of China (Grants No. 12088101, No. U1930402, and No. U1930403). Y.-H. Ma acknowledges support from the China Postdoctoral Science Foundation (Grant No. BX2021030).

-
- [1] L. Szilard, Z. Physik **53**, 840 (1929).
 - [2] K. Maruyama, F. Nori, and V. Vedral, Rev. Mod. Phys. **81**, 1 (2009).
 - [3] J. M. Parrondo, J. M. Horowitz, and T. Sagawa, Nature Phys. **11**, 131 (2015).
 - [4] H. Quan, Y. Wang, Y.-x. Liu, C. Sun, and F. Nori, Phys. Rev. Lett. **97**, 180402 (2006).
 - [5] H. Dong, D. Xu, C. Cai, C. Sun, et al., Phys. Rev. E **83**, 061108 (2011).
 - [6] S. W. Kim, T. Sagawa, S. De Liberato, and M. Ueda, Phys. Rev. Lett. **106**, 070401 (2011).
 - [7] C. Cai, H. Dong, C. Sun, et al., Phys. Rev. E **85**, 031114 (2012).
 - [8] R. Landauer, IBM Journal of Research and Development **5**, 183 (1961).
 - [9] E. Joos, H. D. Zeh, C. Kiefer, D. J. Giulini, J. Kupsch, and I.-O. Stamatescu, *Decoherence and the Appearance of a Classical World in Quantum Theory* (Springer Science & Business Media, 2013).
 - [10] H. D. Zeh, Foundations of Physics **1**, 69 (1970).
 - [11] W. H. Zurek, Rev. Mod. Phys. **75**, 715 (2003).
 - [12] M. Schlosshauer, Rev. Mod. Phys. **76**, 1267 (2005).
 - [13] S. Kullback, *Information Theory and Statistics* (Courier Corporation, 1997).
 - [14] S.-W. Li, Phys. Rev. E **96**, 012139 (2017).
 - [15] S. Still, Phys. Rev. Lett. **124**, 050601 (2020).
 - [16] G. E. Crooks, Phys. Rev. E **75**, 041119 (2007).
 - [17] T. Sagawa and M. Ueda, Phys. Rev. Lett. **100**, 080403 (2008).
 - [18] K. Takara, H.-H. Hasegawa, and D. Driebe, Phys. Lett. A **375**, 88 (2010).
 - [19] M. Lostaglio, D. Jennings, and T. Rudolph, Nat. commun. **6**, 1 (2015).
 - [20] S. Deffner, J. P. Paz, and W. H. Zurek, Phys. Rev. E **94**, 010103 (2016).
 - [21] W. Gerlach and O. Stern, Zeitschrift für Physik **9**, 349 (1922).
 - [22] D. Bohm, *Quantum Theory* (Courier Corporation, 2012).
 - [23] D. E. Platt, Am. J. Phys. **60**, 306 (1992).
 - [24] D. J. Griffiths and D. F. Schroeter, *Introduction to Quantum Mechanics* (Cambridge University Press, 2018), ISBN 978-1-107-18963-8.
 - [25] See Supplemental Materials for detailed discussion on the information recording in the Stern-Gerlach experiment (Sec. I); the thermodynamic signature of full finite-time description of quantum Szilard heat engine (Sec. II).
 - [26] M. Esposito, R. Kawai, K. Lindenberg, and C. V. den Broeck, Phys. Rev. Lett. **105**, 150603 (2010).
 - [27] Z.-C. Tu, Chinese Phys. B **21**, 020513 (2012).
 - [28] V. Holubec and A. Ryabov, J. Stat. Mech. **2016**, 073204 (2016), ISSN 1742-5468.
 - [29] N. Shiraishi, K. Saito, and H. Tasaki, Phys. Rev. Lett. **117**, 190601 (2016).
 - [30] V. Cavina, A. Mari, and V. Giovannetti, Phys. Rev. Lett. **119**, 050601 (2017).
 - [31] Y.-H. Ma, D. Xu, H. Dong, and C.-P. Sun, Phys. Rev. E **98**, 042112 (2018).
 - [32] H. Everett III, Rev. Mod. Phys. **29**, 454 (1957).
 - [33] R. B. Griffiths, J. Stat. Phys. **36**, 219 (1984).
 - [34] P. Mittelstaedt, *The Interpretation of Quantum Mechanics and the Measurement Process* (Cambridge University Press, 2004).
 - [35] A. E. Allahverdyan, R. Balian, and T. M. Nieuwenhuizen, Physics Reports **525**, 1 (2013).
 - [36] Y.-H. Ma, D. Xu, H. Dong, and C.-P. Sun, Phys. Rev. E **98**, 022133 (2018).
 - [37] P. Abiuso and M. Perarnau-Llobet, Phys. Rev. Lett. **124**, 110606 (2020).
 - [38] G. E. Crooks, Phys. Rev. Lett. **99** (2007).
 - [39] Y.-H. Ma, J.-F. Chen, C. P. Sun, and H. Dong, Phys. Rev. E **106**, 034112 (2022).
 - [40] M. J. Ondrechen, B. Andresen, M. Mozurkewich, and R. S. Berry, American Journal of Physics **49**, 681 (1981).
 - [41] Y. Izumida and K. Okuda, Phys. Rev. Lett. **112**, 180603 (2014).
 - [42] Y.-H. Ma, Entropy **22**, 1002 (2020).

- [43] H. Yuan, Y.-H. Ma, and C. Sun, Phys. Rev. E **105**, L022101 (2022).
- [44] Y.-H. Ma, S.-H. Su, and C.-P. Sun, Phys. Rev. E **96**, 022143 (2017).
- [45] W. H. Zurek, Nature Phys. **5**, 181 (2009).
- [46] C. J. Riedel, W. H. Zurek, and M. Zwolak, Phys. Rev. A **93**, 032126 (2016).
- [47] S.-W. Li, C. Cai, X. Liu, and C. Sun, Found. Phys. **48**, 654 (2018).

Supplementary Materials for “Finite-Time Optimization of Quantum Szilard heat engine”

Tan-Ji Zhou

Graduate School of China Academy of Engineering Physics,
No. 10 Xibeiwang East Road, Haidian District, Beijing, 100193, China and
Department of Physics, Peking University

Yu-Han Ma^{*}

Department of Physics, Beijing Normal University, Beijing 100875, China and
Graduate School of China Academy of Engineering Physics,
No. 10 Xibeiwang East Road, Haidian District, Beijing, 100193, China

C. P. Sun[†]

Graduate School of China Academy of Engineering Physics,
No. 10 Xibeiwang East Road, Haidian District, Beijing, 100193, China and
Beijing Computational Science Research Center, Beijing 100193, China

This document is devoted to providing the detailed derivations and the supporting discussions to the main content of the Letter. In Sec. I, we discuss the information recording in the Stern-Gerlach experiment and obtain the spatial wave function, overlapping integral of the wave functions, the conditional spatial distribution probability and the correlation (mutual entropy $I(\hat{t})$) between MD and the spatial state of the particle. In Sec. II, we calculate the EMP of the Szilard heat engine in more general cases with full finite time description of the cycle.

I. INFORMATION RECORDING IN THE STERN-GERLACH EXPERIMENT

The Schematic illustration of the Stern-Gerlach experiment [1–4] is shown in Fig. 1. Non-interacting particles with mass m , momentum p , and magnetic moment $\vec{\mu}$ are injected along z direction with velocity v_z . Physically, the applied inhomogeneous magnetic field $B(x)$ along x direction causes entanglement between the spin and the spatial degrees of freedom of the particles. Such entanglement leads to quantum correlation between these two kinds of degrees of freedom.

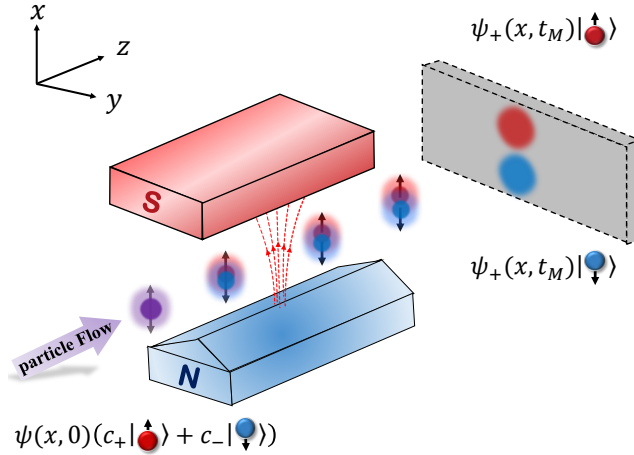


Figure 1: Schematic illustration of Stern-Gerlach experiment. The inhomogeneous magnetic field along x direction results in the entanglement between the spin degrees of freedom and the spatial degrees of freedom of the particles, and thus separate particles with different spins in space.

^{*} yhma@bnu.edu.cn

[†] suncp@gscaep.ac.cn

In the ideal case where the spatial wave packets corresponding to the spin-up and spin-down states of the particle are completely separated, once the state of the spin (spatial) degrees of freedom is determined, the state of the spatial (spin) degrees of freedom can be immediately inferred. Nevertheless, in realistic cases, when the position of the screen for observing the particle distribution is fixed, there is usually overlap between the spatial wave packets associated with different spin states. Intuitively, increasing the movement time of the particle in the magnetic field (or the gradient of the magnetic field) will make the spatial wave packets farther apart along the gradient of the magnetic field, which results in a better distinction between different spin degrees of freedom. In what follows, to quantify the correlation between spin and spatial degrees of freedom, we first study the evolution of the particle's spatial wave packet.

A. Time evolution of the spatial wave packet

The Hamiltonian of the particle reads

$$\hat{H} = \frac{\hat{p}^2}{2m} - \mu_x B(x) \hat{\sigma}_x, \quad (S1)$$

where $\hat{\sigma}_x = (|\uparrow\rangle\langle\uparrow| - |\downarrow\rangle\langle\downarrow|)$ is Pauli matrix in x direction with the corresponding spin up (down) state $|\uparrow\rangle(|\downarrow\rangle)$, and μ_x is the x component of the magnetic moment. Suppose the initial state of particle in spin space and real space are non-entangled, and are respectively $|s\rangle = c_+|\uparrow\rangle + c_-|\downarrow\rangle$ and $|\psi(x, 0)\rangle$, the full initial state of the particle is thus

$$|\Psi(0)\rangle = (c_+|\uparrow\rangle + c_-|\downarrow\rangle) \otimes |\psi(x, 0)\rangle. \quad (S2)$$

In the coordinate representation, one has

$$\langle x|\Psi(0)\rangle = (c_+|\uparrow\rangle + c_-|\downarrow\rangle) \langle x|\psi(x, 0)\rangle. \quad (S3)$$

According to the Schrodinger's equation, the time evolution of total state of the particle follows as

$$\begin{aligned} \langle x|\Psi(t)\rangle &= \langle x|e^{-i\hat{H}t/\hbar}|\Psi(0)\rangle \\ &= c_+\psi_+(x, t)|\uparrow\rangle + c_-\psi_-(x, t)|\downarrow\rangle, \end{aligned} \quad (S4)$$

where $\psi_+(x, t)$ and $\psi_-(x, t)$ are the normalized spatial wave function corresponding to spin state $|\uparrow\rangle$ and $|\downarrow\rangle$, respectively. Without loss of generality, we focus on the the symmetric case that the superposition coefficients of the initial states are $c_+ = c_- = 1/\sqrt{2}$.

In addition, we assume that the inhomogeneous magnetic field is slowly varying over the range of particle motion, and hence $B(x)$ can be expanded to the first-order of x as $B(x) \approx B(0) + [(\partial B/\partial x)|_{x=0}]x$ [3]. In this sense, the Hamiltonian in Eq. (S1) is approximated as

$$\hat{H} = \frac{\hat{p}^2}{2m} - fx\hat{\sigma}_x, \quad (S5)$$

where $f \equiv \mu_x(\partial B/\partial x)|_{x=0}$ is the magnetic force applied on the particle in classical picture. The spatial wave function can be expressed with the path integral approach as [5]

$$\psi_{\pm}(x, t) = \int_{-\infty}^{\infty} K_{\pm}(x, t; x', t') \psi(x', t') dx', \quad (S6)$$

where $\psi(x', t')$ is the wave function at space-time coordinate (x', t') , and $K_{\pm}(x, x'; t)$ is the propagator determined by the Hamiltonian of the system. In our case, without loss of generality, we set initial time $t' = 0$, and choose the initial wave packet as a Gaussian wave packet with width a as

$$\psi(x', 0) \equiv \langle x|\psi(x', 0)\rangle = \left(\frac{1}{2\pi a^2}\right)^{1/4} e^{-\frac{x'^2}{4a^2}}. \quad (S7)$$

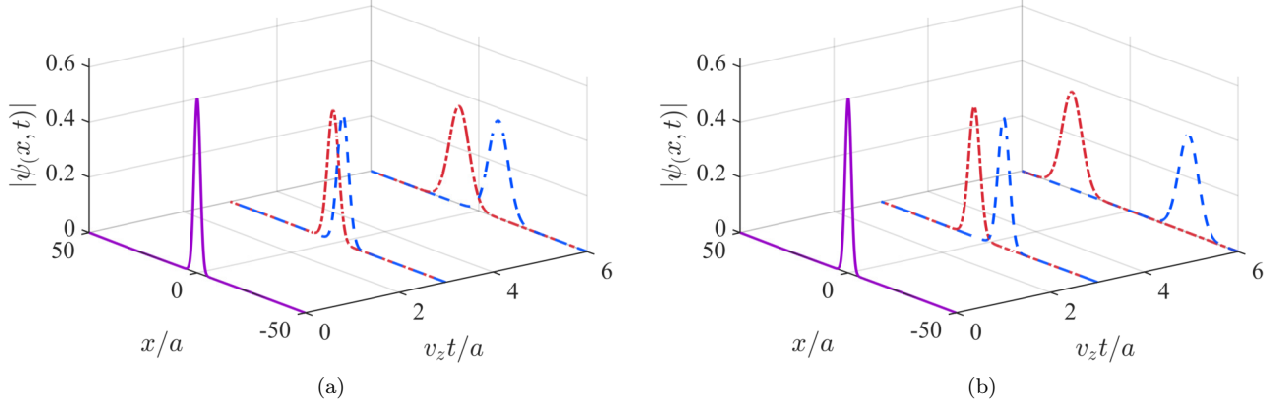


Figure 2: Evolution of the spatial wave packet with $f = 0.5$ (a) and $f = 1.5$ (b). The purple solid curve represents the initial wave packet in Eq. (S7). The red dash-dotted (blue dashed) curves mark $|\psi_+(x, t)|$ ($|\psi_-(x, t)|$) at $t = 3$ and $t = 6$. In this figure, we choose $a = m = \hbar = 1$, the velocity of the particle in the z axis is set to $v_z = 1$.

which is plotted in Fig. 2 as the purple solid curve in the $z = 0$ plane. Note that the Hamiltonian in Eq. (S5) can be reduced to the coordinate space as

$$\hat{H}_+^s \equiv \langle \uparrow | \hat{H} | \uparrow \rangle = \frac{\hat{p}^2}{2m} - f\hat{x}, \quad \hat{H}_-^s \equiv \langle \downarrow | \hat{H} | \downarrow \rangle = \frac{\hat{p}^2}{2m} + f\hat{x}, \quad (\text{S8})$$

the propagator $K_{\pm}(x, x'; t) \equiv \langle x | \exp(-i\hbar^{-1} \int_0^t \hat{H}_{\pm}^s dt) | x' \rangle$ associated with this linear potential reads [5, 6]

$$K_{\pm}(x, x'; t) = \sqrt{\frac{m}{2\pi i \hbar t}} \exp\left(-\frac{m(x-x')^2}{2i\hbar t} \pm \frac{f(x+x')t}{2i\hbar} + \frac{f^2 t^3}{24i\hbar m}\right). \quad (\text{S9})$$

Substituting Eqs. (S9) and (S7) into Eq. (S6), the wave function is obtained as

$$\begin{aligned} \psi_{\pm}(x, t) &= \left(\frac{1}{2\pi a^2}\right)^{1/4} \sqrt{\frac{m}{2\pi i \hbar t}} \int_{-\infty}^{\infty} \exp\left(-\frac{m(x-x')^2}{2i\hbar t} \pm \frac{f(x+x')t}{2i\hbar} + \frac{f^2 t^3}{24i\hbar m}\right) e^{-\frac{x'^2}{4a^2}} dx', \\ &= \left(\frac{1}{2\pi a^2}\right)^{1/4} \sqrt{\frac{m}{2\pi i \hbar t}} \int_{-\infty}^{\infty} \exp\left(-\frac{x'^2}{4a^2} - \frac{m(x-x')^2}{2i\hbar t} \pm \frac{f(x+x')t}{2i\hbar} + \frac{f^2 t^3}{24i\hbar m}\right) dx'. \end{aligned} \quad (\text{S10})$$

Using the one-dimensional Gaussian integral

$$\int_{-\infty}^{\infty} e^{-bz^2 + cz} dz = \sqrt{\frac{\pi}{b}} \exp\left(\frac{c^2}{4b}\right), \quad \text{Re}(b) > 0, \quad (\text{S11})$$

the spatial wave function is straightforward calculated as

$$\psi_{\pm}(x, t) = \frac{(a^2/2\pi)^{1/4}}{\sqrt{a^2 + i\hbar t/2m}} \exp\left\{-\frac{if^2 t^3}{6\hbar m} - \frac{[x \mp ft^2/(2m)]^2}{4(a^2 + i\hbar t/2m)} \pm \frac{iftx}{\hbar}\right\}, \quad (\text{S12})$$

The norms of the above wave functions at $t = 0, 3, 6$ are illustrated in Fig. 2, where (a) is plotted with $f = 0.5$ and (b) is plotted with $f = 1.5$, respectively. All other parameters are set to 1 in this example. The red dash-dotted curves and blue dashed curves are associated with $\psi_+(x, t)$ and $\psi_-(x, t)$, respectively. It is clearly seen in this figure that the degree of separation of the wave packets corresponding to different spin states increases with time. And for a given t , stronger magnetic field gradient, i.e., $f \uparrow$, causes the wave packets to be separated farther apart.

After the measurement process of duration t_M , the spacial overlapping integral $F \equiv |\langle \psi_+ | \psi_- \rangle|$ is

$$\begin{aligned}
F(t_M) &= \int_{-\infty}^{\infty} \psi_+^*(x, t_M) \psi_-(x, t_M) dx \\
&= \frac{(a^2/2\pi)^{1/2}}{\sqrt{a^4 + \hbar^2 t_M^2/4m^2}} \int_{-\infty}^{\infty} \exp \left\{ -\frac{[x - ft_M^2/(2m)]^2}{4(a^2 - i\hbar t_M/2m)} - \frac{[x + ft_M^2/(2m)]^2}{4(a^2 + i\hbar t_M/2m)} - 2\frac{ift_M x}{\hbar} \right\} dx \\
&= \frac{(a^2/2\pi)^{1/2}}{\sqrt{a^4 + \hbar^2 t_M^2/4m^2}} \int_{-\infty}^{\infty} \exp \left\{ -\frac{a^2(x^2 + f^2 t_M^4/4m^2) - i\hbar f x t_M^3/2m^2}{2(a^4 + \hbar^2 t_M^2/4m^2)} - 2\frac{ift_M x}{\hbar} \right\} dx, \tag{S13}
\end{aligned}$$

which is straightforward calculated as, by using Eq. (S11),

$$F(\tilde{t}) = \exp \left[- \left(2\alpha^2 \tilde{t}^2 + \frac{\alpha^2 \tilde{t}^4}{8} \right) \right]. \tag{S14}$$

Here, $\tilde{t} \equiv t_M/\tau_M$ is the dimensionless measurement time, $\tau_M \equiv ma^2/\hbar$ is the characteristic time of the measurement process. $\alpha \equiv ma^3 f/\hbar^2$, which characterizes the strength of decoherence after measurement, is proportional to the magnetic force f . For given \tilde{t} , a stronger magnetic field (larger f) results in a smaller $F(t_M)$, i.e. a more pronounced decoherence corresponds to farther apart wave packets in Fig. 2. Obviously, $F(\tilde{t}) \rightarrow 0$ in the long-time limit $\tilde{t} \rightarrow \infty$ of the measurement process. In this case, there is no overlapping between $\psi_+(x, t)$ and $\psi_-(x, t)$, and the spin of the particle can be perfectly distinguished by observing its spatial wave function in x direction. Therefore, an ideal measurement of the spin is achieved in the Stern-Gerlach experiment.

B. Conditional spatial distribution probability

To discuss the non-ideal measurement within finite measuring duration, we first study the conditional probability $p(L|\uparrow)$ that a spin-up particle appears in the “left” area of the screen, and the conditional probability $p(R|\downarrow)$ that a spin-down particle appears in the right” area of the screen. Here, left and right are divided with respect to the x -direction, which corresponds to the area with $x > 0$ and $x < 0$, respectively. By definitions, the probabilities are

$$\begin{aligned}
p(L|\uparrow) &\equiv \int_0^{\infty} \langle x | [\langle \uparrow | \Psi(t) \rangle \langle \Psi(t) | \uparrow \rangle] | x \rangle dx \\
&= \int_0^{\infty} |\psi_+(x, t_M)|^2 dx, \tag{S15}
\end{aligned}$$

and

$$\begin{aligned}
p(R|\downarrow) &\equiv \int_{-\infty}^0 \langle x | [\langle \downarrow | \Psi(t) \rangle \langle \Psi(t) | \downarrow \rangle] | x \rangle dx \\
&= \int_{-\infty}^0 |\psi_-(x, t_M)|^2 dx. \tag{S16}
\end{aligned}$$

Obviously, due to the symmetry of the spatial wave functions obtained in Eq. (S12), the above two probabilities equals to each other, i.e., $p(L|\uparrow) = p(R|\downarrow) \equiv p(t_M)$. Substituting Eq. (S12) into Eq. (S15) yields

$$\begin{aligned}
p(t_M) &= \int_0^{\infty} |\psi_+(x, t_M)|^2 dx \\
&= \frac{(a^2/2\pi)^{1/2}}{\sqrt{a^4 + \hbar^2 t_M^2/4m^2}} \int_0^{\infty} \exp \left[-\frac{a^2}{2(a^4 + \hbar^2 t_M^2/4m^2)} \left(x - \frac{ft_M^2}{2m} \right)^2 \right] dx \\
&= \frac{(a^2/2\pi)^{1/2}}{\sqrt{a^4 + \hbar^2 t_M^2/4m^2}} \int_{-\frac{ft_M^2}{2m}}^{\infty} \exp \left[-\frac{a^2}{2(a^4 + \hbar^2 t_M^2/4m^2)} y^2 \right] dy \tag{S17}
\end{aligned}$$

Using the Gauss error function

$$\operatorname{erf}(z) \equiv \frac{2}{\sqrt{\pi}} \int_0^z e^{-u^2} du, \quad (\text{S18})$$

we simplify Eq. (S17) as

$$p(t_M) = p(\tilde{t}) = \frac{1}{2} \left[1 + \operatorname{erf} \left(\frac{\alpha \tilde{t}^2}{\sqrt{2\tilde{t}^2 + 8}} \right) \right], \quad (\text{S19})$$

where $\operatorname{erf}(z) = 2\pi^{-1/2} \int_0^z \exp(-u^2) du$ is the Gauss error function. When the dimensionless measurement time \tilde{t} approaches infinity and zero we have $\lim_{\tilde{t} \rightarrow \infty} p(\tilde{t}) = 1$ and $\lim_{\tilde{t} \rightarrow 0} p(\tilde{t}) = 1/2$, respectively. Correspondingly, the probability of a spin-up particle appears in the “left” area, and the probability of a spin-down particle appears in the “right” area are

$$p(R|\uparrow) = \int_{-\infty}^0 |\psi_+(x, t_M)|^2 dx = 1 - p(\tilde{t}), \quad (\text{S20})$$

and

$$p(L|\downarrow) = \int_0^{\infty} |\psi_-(x, t_M)|^2 dx = 1 - p(\tilde{t}). \quad (\text{S21})$$

Here the normalized condition for conditional probabilities $p(L|\theta) + p(R|\theta) = 1, \theta \in \{\uparrow, \downarrow\}$ has been used.

In the long-time regime of $\tilde{t} \gg 1$, we have $p(\tilde{t}) \rightarrow 1$, which results in the conditional probabilities $p(L|\uparrow) = p(R|\downarrow) \rightarrow 1$. In this case, we can achieve an ideal measurement for the spin state through the measurement of the space state: when a particle is observed to be on the left (right) side of the screen, we can definitely determine that its spin state is $|\uparrow\rangle$ ($|\downarrow\rangle$). Conversely, we can also determine the spatial position of a particle by measuring its spin state. However, for an arbitrary \tilde{t} away from the long-time regime, even if the spin state of the particle has been accurately obtained, we can only infer the spatial state of the particle probabilistically. For example, when we find the spin state of the particle is $|\uparrow\rangle$, we therefore infer that the particle is on the left side of the screen. According to Eq. (S20), the probability that this inference is correct is $p_c = p(\tilde{t})$. On the contrary, the probability of this inference being wrong is $p_w = 1 - p(\tilde{t})$, which corresponds to the case where the particle is actually on the right side of the screen.

C. Measurement ideality

As we mentioned in the main text, the measurement of the position of the particle by MD is realized through the detection of the spin state. After the measurement, we assume that the instrument detects the spin perfectly, then the MD state $|D_\theta\rangle$ becomes the relative state of the spin state $|\theta\rangle$, and the conditional probability of spin state given MD state $p(\theta|D)$ satisfies

$$p(\uparrow|D_\uparrow) = p(\downarrow|D_\downarrow) = 1, p(\uparrow|D_\downarrow) = p(\downarrow|D_\uparrow) = 0 \quad (\text{S22})$$

If the observation time is not long enough (in comparison with τ_M), the quantum measurement of the position of the particle is non-ideal. We quantify the correlation information of the demon and the particle with the mutual entropy [7–11]

$$I = S_P + S_D - S_{DP}. \quad (\text{S23})$$

Here, $S_Y = -\sum_{y \in Y} p(y) \ln p(y)$ is the Shannon entropy with respect to the variable Y , $S_{DP} = -\sum_P \sum_D p(P, D) \ln p(P, D)$ is the joint entropy of the particle and the demon, where the joint probability is $p(P, D) = p(P|D)p(D)$. Using such definition and Eqs. (S20) and (S21), the mutual information is obtained as

$$\begin{aligned}
I &= S_P + S_D - S_{DP} \\
&= \sum_{P \in \{R, L\}} \sum_{D \in \{D_\uparrow, D_\downarrow\}} p(P, D) \log \frac{p(P|D)}{p(P)}
\end{aligned}$$

$$= \sum_{P \in \{R, L\}} \sum_{D \in \{D_\uparrow, D_\downarrow\}} \sum_{\theta \in \{\uparrow, \downarrow\}} p(P|D)p(D) \log \frac{p(P|D)}{p(P)} \quad (\text{S24})$$

$$= \sum_{P \in \{R, L\}} \sum_{D \in \{D_\uparrow, D_\downarrow\}} \sum_{\theta \in \{\uparrow, \downarrow\}} p(P|\theta)p(\theta|D)p(D) \log \frac{p(P|\theta)p(\theta|D)}{p(P)} \quad (\text{S25})$$

$$\begin{aligned}
&= p(R|\uparrow)p(\uparrow) \log \frac{p(R|\uparrow)}{p(R)} + p(R|\downarrow)p(\downarrow) \log \frac{p(R|\downarrow)}{p(R)} + p(L|\uparrow)p(\uparrow) \log \frac{p(L|\uparrow)}{p(L)} + p(L|\downarrow)p(\downarrow) \log \frac{p(L|\downarrow)}{p(L)} \\
&= \ln 2 + p(\tilde{t}) \ln p(\tilde{t}) + [1 - p(\tilde{t})] \ln [1 - p(\tilde{t})], \quad (\text{S26})
\end{aligned}$$

where $p(\uparrow) = p(\downarrow) = 1/2$ has been used according to the symmetric choice of superposition coefficients in the initial states.

According to the above equation and Eq. (S19), for the example shown in Fig. 2 (a) with $f = 0.5$, $I_{\tilde{t}=3} = 0.355$ and $I_{\tilde{t}=6} = 0.677$; while for Fig. 2 (b) with $f = 1.5$, $I_{\tilde{t}=3} = 0.692$ and $I_{\tilde{t}=6} = 0.693$. Moreover, we define the measurement ideality as $\mathcal{M}(\tilde{t}) \equiv I(\tilde{t})/\ln 2$, namely,

$$\mathcal{M}(\tilde{t}) = 1 + \frac{p(\tilde{t}) \ln p(\tilde{t}) + [1 - p(\tilde{t})] \ln [1 - p(\tilde{t})]}{\ln 2} \quad (\text{S27})$$

which is illustrated in Fig. 2 of the main text.

The long-time and short-time behaviors of the mutual entropy are discussed below. In the long-time regime of $\tilde{t} \gg 1$, we have $p(\tilde{t}) \rightarrow 1$, keeping to the first order of $1 - p(\tilde{t})$, we have

$$\begin{aligned}
\mathcal{M}(\tilde{t} \gg 1) &\approx 1 + \frac{\ln [1 + p(\tilde{t}) - 1]}{\ln 2} \\
&\approx 1 + \frac{p(\tilde{t}) - 1}{\ln 2} \\
&= 1 + \frac{1}{2 \ln 2} \left[\operatorname{erf} \left(\frac{\alpha \tilde{t}^2}{\sqrt{8 + \tilde{t}^2}} \right) - 1 \right] \\
&\approx 1 - \frac{1 - \operatorname{erf}(\alpha \tilde{t})}{2 \ln 2}. \quad (\text{S28})
\end{aligned}$$

On the other hand, in the short-time regime of $\tilde{t} \ll 1$, we have

$$\begin{aligned}
p(\tilde{t} \ll 1) &= \frac{1}{2} \left[1 + \operatorname{erf} \left(\frac{\alpha \tilde{t}^2}{\sqrt{8 + \tilde{t}^2}} \right) \right] = \frac{1}{2} + \frac{1}{\sqrt{\pi}} \int_0^{\frac{\alpha \tilde{t}^2}{\sqrt{8 + \tilde{t}^2}}} e^{-u^2} du \\
&\approx \frac{1}{2} + \frac{1}{\sqrt{\pi}} \int_0^{\frac{\alpha \tilde{t}^2}{2\sqrt{2}}} (1 - u^2) du \\
&\approx \frac{1}{2} + \frac{\alpha \tilde{t}^2}{2\sqrt{2\pi}}. \quad (\text{S29})
\end{aligned}$$

Then the mutual entropy is approximated as

$$\begin{aligned}
\mathcal{M}(\tilde{t} \ll 1) &= 2 + \left(\frac{1}{2\ln 2} + \frac{\alpha \tilde{t}^2}{2\ln 2 \sqrt{2\pi}} \right) \ln \frac{\frac{1}{2} + \frac{\alpha \tilde{t}^2}{2\sqrt{2\pi}}}{2} + \left(\frac{1}{2\ln 2} - \frac{\alpha \tilde{t}^2}{2\ln 2 \sqrt{2\pi}} \right) \ln \left[\frac{\frac{1}{2} - \frac{\alpha \tilde{t}^2}{2\sqrt{2\pi}}}{2} \right] \\
&= \left(\frac{1}{2\ln 2} + \frac{\alpha \tilde{t}^2}{2\ln 2 \sqrt{2\pi}} \right) \ln \left(1 + \frac{\alpha \tilde{t}^2}{\sqrt{2\pi}} \right) + \left(\frac{1}{2\ln 2} - \frac{\alpha \tilde{t}^2}{2\ln 2 \sqrt{2\pi}} \right) \ln \left(1 - \frac{\alpha \tilde{t}^2}{\sqrt{2\pi}} \right) \\
&\approx \left(\frac{1}{2\ln 2} + \frac{\alpha \tilde{t}^2}{2\ln 2 \sqrt{2\pi}} \right) \left[\frac{\alpha \tilde{t}^2}{\sqrt{2\pi}} - \frac{1}{2} \left(\frac{\alpha \tilde{t}^2}{\sqrt{2\pi}} \right)^2 \right] + \left(\frac{1}{2\ln 2} - \frac{\alpha \tilde{t}^2}{2\ln 2 \sqrt{2\pi}} \right) \left[-\frac{\alpha \tilde{t}^2}{\sqrt{2\pi}} - \frac{1}{2} \left(\frac{\alpha \tilde{t}^2}{\sqrt{2\pi}} \right)^2 \right] \\
&= \frac{\alpha^2 \tilde{t}^4}{8\pi \ln 2} = \frac{m^2 a^6 f^2 \tilde{t}^4}{8\pi \ln 2 \hbar^4},
\end{aligned} \tag{S30}$$

which is proportional to \tilde{t}^4 . The proportional coefficient increases with the square of the magnetic force and with the sixth power of the initial width of the wave packet.

II. THERMODYNAMIC SIGNATURE OF FULL FINITE-TIME DESCRIPTION OF QUANTUM SZILARD HEAT ENGINE

In the main text, we mainly focus on the finite-time effect in the measurement process (Stage I). In this section, we discuss the finite-time behaviors of the other processes (Stages II and III) in the engine cycle.

A. Thermodynamic signatures of information recording and information erasing process

In this part, we further consider the finite-time effect in both the information recording and information erasing processes. According to the finite-time Landauer's principle [12–14], the non-ideal erasing process leads to irreversible energy dissipation which is inversely proportional to the erasing time t_E , namely,

$$W_E(t_E) = k_B T_C \ln 2 \left(1 + \frac{C_E}{t_E} \right), \tag{S31}$$

where C_E is a constant determined by specific erasing process [13, 15]. In this manner, we rewrite the total work of the QSE performs in one cycle as

$$W = \mathcal{M}(t_M) k_B T_H \ln 2 - k_B T_C \ln 2 \left(1 + \frac{C_E}{t_E} \right) \tag{S32}$$

Then, the power and efficiency of the information heat engine becomes

$$\eta(t_M, t_E) = \frac{W}{\mathcal{M}(t_M) k_B T_H \ln 2} = 1 - \frac{1 - \eta_C}{\mathcal{M}(t_M) \ln 2} \left(\ln 2 + \frac{C_E}{t_E} \right), \tag{S33}$$

and

$$P(t_M, t_E) = \frac{\mathcal{M}(t_M) k_B T_H \ln 2 - k_B T_C \ln 2 (1 + C_E t_E^{-1})}{t_M + t_E} \tag{S34}$$

Similar to the situation where only the finite-time effect of the information recording process is taken into account, the EMP of the engine in this situation can also exceed the upper limit of the efficiency of low-dissipation Carnot heat engine $\eta_+ = \eta_C / (2 - \eta_C)$ at certain range of η_C . In order to quantify the influence of parameters α and C_E on the EMP, in Fig. 3, we show the width of the range of η_C within which EMP can exceed η_+ in the two-dimensional parameter space (α, C_E) . It can be seen from the figure that wider range of η_C requires relative large value of α and small value of C_E , which consistent well with physical intuition: for a given operation time, a larger α results in a more complete recording of information, while a smaller C_E corresponds to a more reversible erasing process with less energy dissipation.

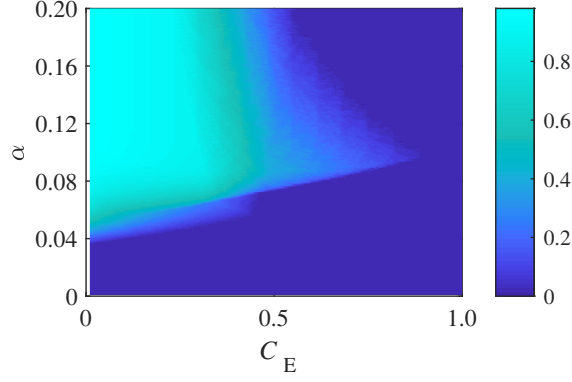


Figure 3: The width of the range of η_C that the efficiency at maximum power (EMP) can exceed η_+ in two-dimensional parameter space (α, C_E) . Lighter area corresponds to wider range of η_C within which EMP can exceed the typical bound of EMP $\eta_+ = \eta_C / (2 - \eta_C)$.

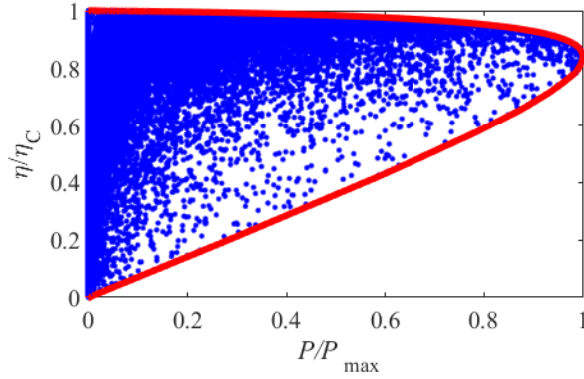


Figure 4: Power-efficiency trade-off relation of the information heat engine, where the finite-time effects of both the information recording and information erasing process are considered. The Blue dots are obtained numerically from

Eqs. (S33) and (S34) with 10^7 sets of measurement time and erasing time pair (\tilde{t}, t_E) chosen randomly from $\tilde{t} \in (1, 4)$ and $t_E \in (1, 400)$. The Red solid curve marks the envelop of these blue dots, namely, the boundary of the power-efficiency trade-off. In this plot, we choose $\eta_C = 0.6$, $\alpha = 0.4$ and $C_E = 0.5$.

The power-efficiency trade-off relation is shown in Fig. 4 by calculating the efficiency η/η_C and the power P/P_{\max} corresponding to 10^7 of random measurement time and erasing time pairs (\tilde{t}, t_E) from (1, 1) to (4, 400). Each blue dot in Fig. 4 represents a heat engine cycle with different (\tilde{t}, t_E) , and the red solid curve is the envelop of these blue dots which shows the boundary of the trade-off relation. Different from the single-variable case shown in Fig. 5(b) in the main text where the system can only operate with power and efficiency locate on the curve, the heat engine with the finite-time effects in both the information recording and information erasing processes taken into consideration can operate at anywhere within the envelop. The efficiency at an arbitrary given power P_a is bounded by two intersection points of the vertical line $P = P_a$ and the red solid curve. As $P/P_{\max} \rightarrow 0$, η/η_C approaches 1, which covers the quasi-static regime of the information heat engine.

B. Thermodynamic signature of work outputting and information erasing process

In the last case to be studied, we assume $\tau_M \ll t_M \ll t_O(t_E)$. In this regime, the information recording is complete with $\mathcal{M}(t_M) \approx 1$, and operation time of the measurement process can be ignored in comparison with that of the work outputting and information erasing process. Below, we focus on the EMP of the information engine.

In the work outputting process, the information engine is contact with a heat reservoir of temperature T_H , and such a process is the same as the finite-time isothermal process in the Carnot-like cycle [16–19]. In the low-dissipation regime [18–22], the output work follows as

$$W_O(t_O) = T_H \Delta S \left(1 - \frac{C_O}{t_O}\right), \quad (\text{S35})$$

where $\Delta S = k_B \ln 2$ is the reversible entropy change [23, 24] and C_O is the dissipation constant. It follows from Eqs. (S35) and (S32) that the power of engine becomes a function of t_O and t_E as

$$P(t_O, t_E) = \frac{W_O(t_O) - W_E(t_E)}{t_O + t_E} \quad (\text{S36})$$

$$= T_H \Delta S \frac{\eta_C - C_O t_O^{-1} - (1 - \eta_C) C_E t_E^{-1}}{t_O + t_E}. \quad (\text{S37})$$

It is easy to check that the maximum power $P = P_{\max}$ is achieved when $\partial P / \partial t_O = 0$ and $\partial P / \partial t_E = 0$, and the optimal operation times at maximum power are obtained as

$$t_O^* = \frac{2C_O}{\eta_C} \left(1 + \sqrt{\frac{C_E}{C_O}}\right), \quad t_E^* = t_O^* \sqrt{\frac{C_E}{C_O}} \quad (\text{S38})$$

Correspondingly, the efficiency at maximum power (EMP) for this information engine is

$$\eta_{MP} = 1 - \frac{W_E(t_E^*)}{W_O(t_O^*)} = \frac{\eta_C}{2 - \kappa \eta_C}. \quad (\text{S39})$$

Here $\kappa = \left[1 + \sqrt{C_E / (C_O)}\right]^{-1}$ depends on the asymmetry of dissipation when the heat engine is in contact with two heat reservoirs. Since $0 \leq \kappa \leq 1$ for different Σ_c / Σ_h , η_{MP} is found to satisfy the following inequality

$$\eta_L \equiv \frac{\eta_C}{2} \leq \eta_{MP} \leq \frac{\eta_C}{2 - \eta_C} \equiv \eta_U. \quad (\text{S40})$$

In the above relation, η_U and η_L are respectively the upper and lower bound of EMP.

Equation (S40) covers the result obtained with the low-dissipation model for finite-time Carnot engine [18]. This indicates that when the information recording is ideal and the corresponding duration is ignored, the finite-time Szilard engine is mapped to a low-dissipation Carnot heat engine. When the dissipation coefficients in the work outputting process and information erasing process are the same as each other, i.e., $C_E / C_O = 1$, the EMP of Eq. (S39) recovers the so-called Curzon-Ahlborn efficiency, i.e., $\eta_{CA} = 1 - \sqrt{T_C / T_H}$ [16].

-
- [1] W. Gerlach and O. Stern, *Zeitschrift für Physik* **9**, 349 (1922).
 - [2] D. Bohm, *Quantum Theory* (Courier Corporation, 2012).
 - [3] D. E. Platt, *Am. J. Phys.* **60**, 306 (1992).
 - [4] D. J. Griffiths and D. F. Schroeter, *Introduction to Quantum Mechanics* (Cambridge University Press, 2018), ISBN 978-1-107-18963-8.
 - [5] R. P. Feynman, A. R. Hibbs, and D. F. Styer, *Quantum Mechanics and Path Integrals* (Courier Corporation, 2010), ISBN 978-0-486-47722-0.
 - [6] B. C. Hsu, M. Berrondo, and J.-F. S. Van Huel, *Phys. Rev. A* **83**, 012109 (2011).
 - [7] S. Kullback, *Information Theory and Statistics* (Courier Corporation, 1997).
 - [8] M. A. Nielsen and I. L. Chuang, *Quantum Computation and Quantum Information* (Cambridge University Press, 2002).
 - [9] S.-W. Li, *Phys. Rev. E* **96**, 012139 (2017).
 - [10] S. Still, *Phys. Rev. Lett.* **124**, 050601 (2020).
 - [11] Y.-H. Ma, C. Liu, and C. Sun, arXiv preprint arXiv:2110.04550 (2021), 2110.04550.
 - [12] A. Bérut, A. Arakelyan, A. Petrosyan, S. Ciliberto, R. Dillenschneider, and E. Lutz, *Nature* **483**, 187 (2012).
 - [13] K. Proesmans, J. Ehrlich, and J. Bechhoefer, *Phys. Rev. Lett.* **125**, 100602 (2020).
 - [14] Y.-H. Ma, J.-F. Chen, C. Sun, and H. Dong, *Physical Review E* **106**, 034112 (2022).
 - [15] Y.-H. Ma, J.-F. Chen, C. P. Sun, and H. Dong, *Phys. Rev. E* **106**, 034112 (2022).

- [16] F. L. Curzon and B. Ahlborn, Am. J. Phys. **43**, 22 (1975).
- [17] T. Schmiedl and U. Seifert, EPL (Europhysics Lett.) **83**, 30005 (2008).
- [18] M. Esposito, R. Kawai, K. Lindenberg, and C. V. den Broeck, Phys. Rev. Lett. **105**, 150603 (2010).
- [19] Y.-H. Ma, D. Xu, H. Dong, and C.-P. Sun, Phys. Rev. E **98**, 042112 (2018).
- [20] Y.-H. Ma, D. Xu, H. Dong, and C.-P. Sun, Phys. Rev. E **98**, 022133 (2018).
- [21] P. Abiuso and M. Perarnau-Llobet, Phys. Rev. Lett. **124**, 110606 (2020).
- [22] Y.-H. Ma, R.-X. Zhai, J. Chen, C. Sun, and H. Dong, Phys. Rev. Lett. **125**, 210601 (2020).
- [23] H. Dong, D. Xu, C. Cai, C. Sun, et al., Phys. Rev. E **83**, 061108 (2011).
- [24] S. W. Kim, T. Sagawa, S. De Liberato, and M. Ueda, Phys. Rev. Lett. **106**, 070401 (2011).